(15) Uehara, K.; Nitta, K.; Sugai, S. *Polymer* **1979**, *20*, 670.
(16) Tiffany, L. M.; Krimm, S. *Biopolymers* **1972**, *11*, 2309.
(17) Miyazaki, M.; Yoneyama, M.; Sugai, S. *Polymer* **1978**, *19*, 995.
(18) Barbucci, R.; Casolaro, M.; Ferruti, P.; Nocentini, M.; Macromolecules **1986**, *19*, 1856.
(19) Doty, P.; Wada, A.; Yang, J. T.; Blout, E. R. *J. Polym. Sci.* **1957**, *23*, 851.
(20) Blout, E. R.; Asadourian, A. *J. Am. Chem. Soc.* **1956**, *78*, 955.
(21) Pearson, J. F.; Slifkin, M. A. *Spectrochim. Acta, Part A* **1972**, *28A*, 2403.

Interfacial Structure and Dynamics of Macromolecular Liquids: A Monte Carlo Simulation Approach

Kevin F. Mansfield and Doros N. Theodorou*

Department of Chemical Engineering, University of California, Berkeley, California 94720, and Center for Advanced Materials, Lawrence Berkeley Laboratory, Berkeley, California 94720. *Received October 14, 1988; Revised Manuscript Received December 28, 1988*

ABSTRACT: Dynamic Monte Carlo simulations are performed on a dense liquid consisting of freely jointed, 20-bead long chain molecules in a cubic lattice in the vicinity of solid walls. The objective is to elucidate the equilibrium structure and dynamic behavior of polymer melts at interfaces. Elementary bead moves are chosen so as to mimic the process of conformational isomerization. Three different solid surfaces are studied: (I) a strongly attractive surface with high potential barriers between adsorption sites that inhibit the lateral motion of adsorbed beads; (II) an equally strongly attractive surface with no barriers; (III) a weakly attractive surface with low potential barriers between sites. The microscopic structure of the polymeric liquid is significantly affected by the presence of solid walls. Segment density is enhanced near the strongly attractive surfaces and depleted near the weakly attractive surfaces. The distribution of chain centers of mass is peaked at a distance slightly less than one radius of gyration from the solid. Chain shapes are pronouncedly flattened adjacent to a solid wall and gradually assume unperturbed bulk characteristics as one moves away from the wall. The self-diffusion coefficient of chains, evaluated by monitoring their mean-squared center of mass displacement as a function of simulation time, is dramatically reduced near strongly adsorbing walls; on the contrary, chain mobility is enhanced near weakly adsorbing walls. The spatial dependence of self-diffusivity is highly correlated with, but not exclusively governed by, the behavior of local segment density in the interfacial region. The diffusive motion of chains is inherently anisotropic near a surface. Potential barriers between strongly attractive surface sites have only a minor effect on the self-diffusivity. The longest relaxation time of chains is determined as a function of their center of mass position by analyzing the long-time behavior of the end-to-end distance vector autocorrelation function. Strong segment–wall attraction prolongs relaxation times in the surface region appreciably, in comparison to the bulk. Moreover, potential barriers to the lateral motion of adsorbed segments exert a profound influence on the rate of molecular relaxation. Adding such barriers to a strongly attractive surface can cause the relaxation time of chains located near the surface to rise by as much as 80%.

1. Introduction

Interfaces between macromolecular liquids and solids play a key role in many technical applications. Gaining insight into the interfacial structure and dynamics of chain molecules in the solventless, condensed state will enhance our ability to design materials systems with controlled adhesion, wetting, and lubrication characteristics. Recent experimental evidence[1] indicates that substrate/polymer interactions can drastically influence the quality of products obtained by melt processing operations, such as extrusion and film blowing, through the phenomena of wall slip and melt fracture. On a more fundamental level, we wish to understand dynamic surface forces exhibited by neat, low molecular weight polymer liquids confined between closely spaced solid surfaces. Such forces have been measured recently by Horn and Israelachvili.[2]

The equilibrium and dynamic characteristics of a macromolecular liquid in the vicinity of a solid surface are expected to depart significantly from those of the unconstrained bulk. Adsorptive interactions between chain segments and sites on the surface and entropic constraints imposed on the propagation of chains at a phase boundary strongly influence local density, conformation, mobility, and relaxation. All these aspects vary with distance from the solid surface, on a length scale comparable to chain dimensions. The ensuing local property profiles govern the macroscopically manifested interfacial behavior of the polymer liquid.

Previous modeling work on bulk polymers at interfaces has focused on structural and thermodynamic properties. A lattice-based self-consistent mean field approach[3,4] has been useful in predicting bond orientation, chain shape, and density distribution, as well as surface and interfacial tension. A Monte Carlo simulation of the free surface of a polymer melt was recently presented by Madden,[5] who employs a highly efficient pseudokinetic algorithm to sample configuration space; it, too, invokes a lattice representation of the polymer. Lattices afford considerable simplification in dealing with the complicated configuration space of multichain systems, while at the same time they can preserve the basic physics of the problems at hand. More recently, a lattice Monte Carlo simulation has been performed by Ten Brinke et al.[6] on a polymer film confined between two nonadsorbing solid surfaces. Kumar et al.[7] report structural features obtained by Monte Carlo in a similar model system, using a continuum representation of the polymer.

Our interest here is in developing a simulation approach that can provide information not only on structural but also on *dynamic* characteristics of macromolecular liquids

* To whom correspondence should be addressed at the University of California.

0024-9297/89/2222-3143$01.50/0

at interfaces. Metropolis Monte Carlo[8] is an excellent method for obtaining equilibrium properties, provided the elementary moves chosen to explore configuration space result in an ergodic simulation scheme. For the elementary moves used in this work ("end bead", "kink–jump") the question of ergodicity has been addressed by Kremer and Binder;[9] systematic errors due to lack of ergodicity seem to be smaller than the statistical error inherent in the simulations.

The idea that Monte Carlo simulations can yield useful information on the dynamic behavior of macromolecular sysems is due to Verdier and Stockmayer,[10] who first presented a Monte Carlo study of molecular relaxation for short single chains. Kranbuehl and Schardt[11] extended this approach to bulk multichain systems. Dynamic Monte Carlo has been employed in numerous more recent works. Clearly, a Monte Carlo simulation cannot follow the exact temporal evolution of a system; a solution of the dynamic equations governing the system (e.g., Newton's second law of motion, as implemented in the method of molecular dynamics) would be required for this.[12] Nevertheless, useful dynamic information *can* be extracted from Monte Carlo, provided elementary moves are judiciously chosen and a correspondence between attempted moves and actual elapsed time is carefully established. There has been considerable discussion on what elementary moves and what lattice type would best capture the real dynamics of macromolecular systems. Much of this discussion is concerned with the chain-length dependence of relaxation times in the presence of excluded-volume effects.[13-15] The work reported here addresses the question of dynamics in the vicinity of solid surfaces. Our emphasis is on probing how adsorptive interactions and entropic restrictions will affect motion in a model system, whose dynamics in the bulk has been well explored. Our objective is not to analyze the scaling behavior of relaxation times and diffusion with chain length. All simulations reported herein have actually been performed with the same chain size. Elementary moves were selected so as to mimic the process of conformational isomerization through rotation around skeletal bonds. Only the most basic of moves were implemented in order to keep computations tractable. Our semiquantitative conclusions on the position and direction dependence of dynamics in the inherently anisotropic systems explored here are not expected to depend on the particular set of elementary moves or on the lattice representation we employ.

In this work we apply the dynamic Monte Carlo method to a liquid composed of short, linear, flexible chains, confined by adsorbing, impenetrable solid walls. To our knowledge, this is the first time this method has been applied to an interfacial system. Our objectives are (1) to elucidate equilibrium structure and conformation near the solid walls, (2) to study the mobility of chains, by analyzing chain center of mass diffusion as a function of position in the interfacial region, and (3) to understand how molecular relaxation in the bulk is affected by the presence of solid surfaces, by calculating the longest relaxation time of chains at various distances from a surface. We will examine how the adsorptive strength and topography of the solid surface affects the above structural and dynamic properties, within the context of our simple lattice model. Finally, we will compare our interfacial simulations to simulations of the corresponding unconstrained liquid, carried out in the absence of solid surfaces.

2. The Model

Following previous Monte Carlo works[5,10,11] we will represent the polymer as a cubic lattice. Polymer chains are pictured as freely jointed strings of segments, or "beads", occupying adjacent sites in the lattice, while a small fraction of the sites are void, to allow for the compressibility of the polymer. More elaborate lattice representations[16] lead to qualitatively the same results for the properties we are concerned with as does a simple cubic lattice and are therefore not implemented here. A chain length of $r = 20$ beads was used in all our simulations. This is much below the critical entanglement molecular weight of any polymer. To form a thin film of liquid of effectively infinite extent and finite width, periodic boundary conditions are implemented in the x and y directions only. Our model system is a box of dimensions 7 by 7 by 20 lattice spacings in the x, y, and z directions, respectively. The film thickness has been chosen large enough so as to make bridging unlikely and to isolate the effects of the two interfaces. We chose the lattice spacing (edge length of a lattice cell) as a unit for measuring lengths in our model; we will symbolize this elementary length by l. We chose our coordinate system so that planes separating successive lattice layers parallel to the surfaces intersect the z axis at integer coordinates $z/l = i$, $i = 1(1)19$. Thus, bead centers lie at half-integer coordinates $z/l = (i - {}^1/_2)$, $i = 1(1)20$. Two impenetrable solid walls are placed at $z = 0$ and $z = 20l$. Beads adjacent to them, i.e., beads with coordinates $z = 0.5l$ and $z = 19.5l$, will be referred to as "adsorbed".

Segments in a real polymer interact through a distance-dependent potential function. In the vicinity of a solid surface, they also experience a potential energy field due to the solid. In our lattice model, energetics are considerably simplified by introducing four characteristic energies. As in the work of Naghizadeh and Kovac,[17,18] each pair of beads that are not directly bonded but occupy adjacent sites in the lattice, contributes an attractive potential ϵ_b. Short-range repulsion or "excluded-volume" effects are taken into account by incorporating a highly repulsive interaction energy ϵ_x between beads occupying the same site. By lowering the value of ϵ_x we can relax excluded volume, if desired, as has been done in some previous studies.[19,20] In all simulations reported here, ϵ_x is retained very high, so as to preclude the multiple occupancy of sites altogether. The solid surfaces are envisioned as square arrays of adsorption sites. These arrays are commensurate with the polymer lattice, i.e., adsorption sites are centered immediately below (and above) the centers of lattice cells belonging to the first (and twentieth) layers of the model polymer. Polymer/solid interactions are again nearest neighbor. Each adsorbed segment experiences an attractive potential energy well of depth ϵ_a. In addition, neighboring sites on a solid surface are separated by a potential energy barrier, of height ϵ_s. This barrier inhibits the rate of lateral motion of adsorbed segments on the surface. The meaning of the energy parameters ϵ_a and ϵ_s is explained pictorially in Figure 1. It should be emphasized that since polymer segments are constrained to always be aligned with surface sites, the intersite barriers ϵ_s have no influence whatsoever on the thermodynamics of the system. They affect only the rates of transition between system microstates; ϵ_s is thus a purely dynamical quantity, as will be confirmed below. Our consideration of the wells ϵ_a in addition to the barriers ϵ_s constitutes an elementary attempt to incorporate both the adsorptive character (high–low energy) and the topography, or texture of the surface in our model. The latter is of particular interest in conjunction with wall-slip phenomena.

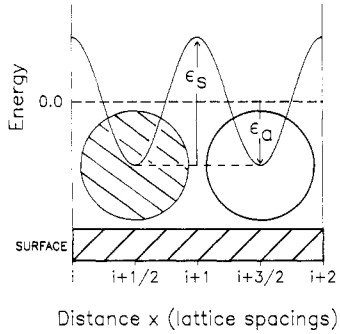

Figure 1. Schematic representation of two characteristic potential energies, associated with the surface. ϵ_a describes the attractive interaction between a surface site and a segment (bead) adsorbed on that site. ϵ_s is an energy barrier, hindering the lateral motion of beads between surface sites.

In establishing a correspondence between our model and real systems, it is useful to compare our parametric representation with that proposed in the equation of state work of Sanchez and Lacombe[21] for linear polyethylene. With their definition of a model segment, the lattice spacing is l = 2.76 Å. All results reported here were obtained at a simulation temperature of T = 200 °C. The attractive bead–bead interaction energy is $\epsilon_b = -0.457k_BT$, where k_B is the Boltzmann constant; this value is consistent with the T^* parameter recommended for polyethylene by Sanchez and Lacombe. The energy penalty for double occupancy of a lattice cell is $\epsilon_x = 12.71k_BT$. With this value, the probability of a double occupancy is only 3×10^{-6}; multiple occupancies were practically never observed during the equilibrium part of our simulations. Our model box contains a total of n = 36 chains. Thus, the average volume fraction of polymer in our lattice is 0.735. This implies a bulk mass density of 0.67 g/cm^3, which is by roughly 10% lower than the density predicted by the Sanchez–Lacombe equation of state for linear polyethylene at 200 °C and 1 atm. This choice of a density lower than experimental was made to enhance the efficiency of the Monte Carlo algorithm. On the other hand, we do not expect that the structural and dynamic results discussed in the following would be drastically affected by this choice at the high densities of interest here.

The effects of the solid surface were studied systematically by performing simulations for three different combinations of ϵ_a and ϵ_s values. Case I is representative of a strongly adsorbing, or "high energy" surface, which at the same time presents strong intersite potential barriers to the lateral movement of segments in the x and y directions. The adhesive attraction (ϵ_a) in case I is roughly 5 times stronger than the bead–bead cohesive interaction (ϵ_b). The barrier height is taken as equal to the adsorptive well depth $|\epsilon_a|$. This means that case I surfaces are quite "corrugated" energetically; i.e., they possess well-expressed adsorption sites. In case II a surface with the same adsorptive strength as in case I is examined. In case II, however, there are no barriers to lateral motion, i.e., the solid is perfectly "smooth". Finally, a surface exhibiting weak attraction toward chain segments and equally weak barriers to lateral motion is studied in case III. The energy parameters for these three cases are summarized in Table I. In presenting results and conclusions, we will often refer to these three situations by case number only.

Most of the computations reported in the following were performed on a VaxStation II, running Ultrix Fortran. Some long runs were undertaken on the San Diego Supercomputer Center's Cray X/MP-48 to ensure convergence of the accumulated averages and to explore possibilities of vectorizing the code, which might allow this work to be extended to much larger chain systems, representative of "real" polymers.

Table I
Summary of Interaction Parameters Used in All Cases Studied[a]

case	$\epsilon_b/(k_BT)$	$\epsilon_x/(k_BT)$	$\epsilon_a/(k_BT)$	$\epsilon_s/(k_BT)$
I	−0.457	12.710	−2.352	2.352
II	−0.457	12.710	−2.352	0.000
III	−0.457	12.710	−0.336	0.336

[a] Simulation temperature T = 473 K.

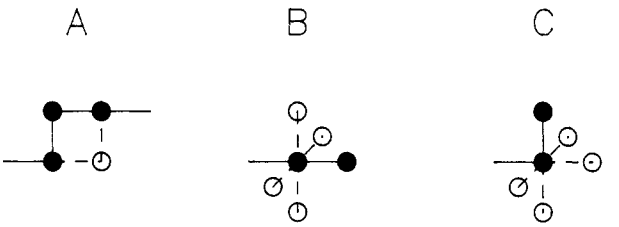

Figure 2. Bead moves attempted during the simulation: (A) there is one possible move for nonterminal beads; (B and C) terminal beads can move into one of four neighboring lattice cells.

3. The Simulation

In a Monte Carlo simulation the configuration space of a system is sampled by generating a Markov chain of microstates. To accomplish this sampling, one needs to define a set of elementary "moves". At each step of the simulation procedure one such move is tried, according to a predetermined set of probabilities of attempt, or frequencies. The attempted move is then evaluated, according to an appropriately chosen set of selection rules and either accepted (which means that the system will assume a new state at the end of the simulation step) or rejected (which means that the state of the system at the end of the simulation step will remain the same as it was at the end of the previous step). Since we are interested in obtaining meaningful dynamic information from our simulations, we must select our elementary moves so as to mimic molecular motion in the actual physical system as realistically as possible. Molecular rearrangement in liquid phases of flexible macromolecules occurs mainly through torsion around skeletal bonds. Following Kranbuehl and Schardt,[11] we have selected three kinds of Monte Carlo moves to represent this process of conformational isomerization, as shown in Figure 2. These are (A) cross corner ("kink–jump") moves of non-end beads, involving a 180° "flip" of a gauche pair of adjacent bonds around the axis connecting their nonshared end points, (B) trans–gauche end-bead moves, involving a 90° bending of a straight-chain tail about the penultimate segment, and (C) gauche–trans and gauche–gauche end-bead moves, involving straightening of a bent-chain tail abount the penultimate segment or rotation of a bent-chain tail around the penultimate bond. (The terms trans and gauche are used here in a simple lattice sense, to denote a pair of adjacent bonds at 180° and 90° to each other, respectively.) Note that the chosen moves prohibit chains from doubling back upon themselves. An additional "crankshaft" type three-bond move has been incorporated in recent Monte Carlo simulations.[9,22,23] It has been established that this move is essential to achieve proper Rouse-like dynamics in the presence of excluded volume. This crankshaft move is not used in this work. In view of the results of Stokely et al.[24] it is felt that it will not affect our conclusions in the regime of short chain lengths and high densities, which we focus on here. We will address the importance of crankshaft motions quantitatively

$$q(i,j) = \begin{cases} \frac{1}{nr} \exp\left\{\frac{-\epsilon_s}{k_B T}\delta[A_i(s_{ij}) + A_j(s_{ij}) - 2]\right\}, & \text{if state } j \text{ is obtained from state } i \text{ through a type A move} \\ \frac{1}{4nr} \exp\left\{\frac{-\epsilon_s}{k_B T}\delta[A_i(s_{ij}) + A_j(s_{ij}) - 2]\right\}, & \text{if state } j \text{ is obtained from state } i \text{ through a type B or C move} \\ 0, & \text{otherwise} \end{cases} \quad (1)$$

in future work. Other schemes, such as the one incorporated in Madden's pseudokinetic algorithm[5] may be more efficient for sampling structural and thermodynamic properties, but highly unrealistic as pictures of the actual temporal evolution of multichain systems in configuration space; they are therefore not implemented here.

Given a state i of our model system, we will symbolize by $q(i,j)$ the (conditional) probability that, in the course of a simulation step, a move will be attempted that takes the system from state i to state j. If τ is the time represented by an attempted move, the quantity $q(i,j)/\tau$ is the intrinsic rate of the elementary process taking the system from state i to state j. In our simulation, moves are attempted as follows: One of the nr beads of the system in state i is selected at random, and all possible moves of this bead, leading to other states j, are evaluated. These moves may be (i) none, if the bead is an internal bead connecting two trans bonds, (ii) one type A move, if the bead is an internal bead connecting two gauche bonds, (iii) four type B moves, if the bead is a terminal bead at the end of a pair of trans bonds, and (iv) four type C moves, if the bead is a terminal bead at the end of a pair of gauche bonds. It is then decided to attempt one of the possible moves. If the selected bead is not adjacent to a surface, either in state i or in the new state, to which the move leads, the attempted move is chosen among all possible moves with equal probability. If, however, the selected bead is adsorbed in both initial and terminal states, which implies that the associated move involves lateral bead displacement on the surface, the probability of this move is reduced by a factor of $\exp[-\epsilon_s/k_B T]$. This is how the effect of intersite barriers on the evolution of the system in configuration space is taken into account. By the above scheme, moves are attempted only between states (i,j) differing in the position of a single bead. Let s_{ij} symbolize that bead. Let also $A_k(s_{ij})$ be an index that assumes a value of 1 if bead s_{ij} in state k is adsorbed and 0 otherwise. The probabilities of attempting a move are given by eq 1. This provides a definition of $q(i,j)$ for $i \neq j$; δ has the usual meaning of a Kronecker δ.

Having decided to attempt a move, taking the system from state i to state j, we now accept or reject that move according to the Metropolis selection rules.[8] Let $E(k)$ be the total energy of the model system in state k, and

$$\Pi(k) = \exp[-E(k)/k_B T] \quad (2)$$

the Boltzmann factor associated with this energy. Let $n_k^{nb}(s_{ij})$ be the number of nonbonded neighbors to the segment s_{ij} in state k. Let also $S_k(s_{ij})$ be the total number of beads in the cell occupied by segment s_{ij}, including segment s_{ij} itself; obviously, $S_k(s_{ij}) \geq 1$. The difference in energy between states i and j is

$$\Delta E(i,j) = E(j) - E(i) = \epsilon_b[n_j^{nb}(s_{ij}) - n_i^{nb}(s_{ij})] + \epsilon_x[S_j(s_{ij}) - S_i(s_{ij})] + \epsilon_a[A_j(s_{ij}) - A_i(s_{ij})] \quad (3)$$

The three terms on the right-hand side account for nearest-neighbor attraction, repulsion due to segment overlap (multiple occupancy), and adsorptive interactions, respectively. If, for the attempted move from i to j, $\Delta E(i,j) \leq 0$, then the move is accepted. If, on the other hand, $\Delta E(i,j) > 0$, then the move is accepted with probability $\Pi(j)/\Pi(i) = \exp[-\Delta E(i,j)/k_B T]$.

With the above rules for attempting and accepting moves, the transition probability matrix used to generate our Markov chain of states is given by

$$p(i,j) = \begin{cases} q(i,j) \min [1, \Pi(j)/\Pi(i)] & i \neq j \\ 1 - \sum_{k \neq i} p(i,k) & i = j \end{cases} \quad (4)$$

where $q(i,j)$ is defined by eq 1, and $\Pi(j)/\Pi(i)$ is obtained from eq 2 and 3. The matrix $\mathbf{q}$, as defined in eq 1, is symmetric. As a consequence, the following condition of microscopic reversibility is satisfied:

$$\Pi(i)\, p(i,j) = \Pi(j)\, p(j,i) \quad (5)$$

This leads directly to[25,26]

$$\sum_i \Pi(i)\, p(i,j) = \Pi(j) \quad (6)$$

In other words, Π is a stationary distribution of the transition matrix $\mathbf{p}$, and our Metropolis scheme will sample asymptotically a distribution of states given by eq 2, i.e., the canonical ensemble. Note that the barriers ϵ_s, while affecting the temporal evolution of our model system in configuration space, leave the distribution sampled at equilibrium (hence, the thermodynamics) unperturbed. The symbol t will denote elapsed time (in seconds). Our dynamic analysis is based upon establishing a correspondence between an attempted move and a time interval, τ. We will use the term "bead cycle" to designate an attempted move. The quantity τ is measured in seconds/bead cycle. The temporal evolution of the system is viewed as a Poisson process, the elementary events in this process being attempts to move individual beads. Simulating such a process in continuous time would be possible.[27] The discretized time approach employed here is satisfactory, given that the characteristic times of the phenomena we wish to focus on (diffusion, relaxation) are much longer than τ. The larger the model system, the smaller the actual time interval that the bead cycle τ represents. The quantity $nr\tau$ is system-size independent and corresponds to a physical time, in seconds. With our choice of elementary moves and temperature and if one is willing to reproduce experimental values of self-diffusivity in the bulk[28] (section 4), one should assign $nr\tau$ a value of approximately 2.3×10^{-15} s. The configuration of the system is monitored at various times, differing from each other by a prespecified number of bead cycles. Running averages are accumulated of all quantities of interest.

A simulation is performed in three stages. Stage 1 is an equilibration stage. It begins with the generation of an initial guess configuration for all chains in the lattice; this first configuration is laid out by hand in our work. Monte Carlo is then performed on the system for at least 100×10^6 bead cycles, to obtain an equilibrium representation of the multichain liquid that is completely free of bead overlaps. Convergence of the mean-squared end-to-end distance and radius of gyration is used as a criterion for sufficient equilibration. Stage 2 aims at obtaining a few quickly converging equilibrium characteristics of the sys-

tem. It consists of taking the configuration reached at the end of stage 1 and further simulating it by Monte Carlo, while at the same time monitoring the structural properties of interest. This part of the simulation requires 8×10^6 bead cycles and runs for approximately 20 min on a VaxStation II. Stage 3 is designed for obtaining dynamic properties. It is a continuation of the second stage, except that now the mobility and relaxation characteristics are monitored, as will be described in detail in section 4. Forming meaningful estimates of dynamic properties is quite demanding computationally. Thus, stage 3 is the most intensive part of the simulation. To enhance its efficiency, this stage was stripped of all equilibrium structure calculations performed in stage 2. Approximately 300×10^6 bead cycles are devoted to stage 3. Stages 1, 2, and 3, as described above, comprise one run for a specific case. Additional runs for the same case consisted of stages 2 and 3 only; in each of them, the final configuration of the previous run (guaranteed to be at equilibrium) served as a new initial guess. A total of seven independent runs were undertaken for each of the three cases studied. The acceptance ratio of attempted moves during a run was approximately 15%. The results plotted in the following section represent averages, accumulated over stage 2 or 3 of all seven runs performed for a given case. Error bars indicate 95% confidence limits.

All features studied are functions of position with respect to the solid surfaces. To correlate results, the lattice was partitioned into $B = 20$ parallel layers, or "bins", of width equal to one lattice spacing along the z direction. Bin Z ($1 \le Z \le B$) extends between $z/l = (Z - 1)$ and $z/l = Z$. The symmetry of the system with respect to the midplane $z/l = 10$ was taken into account, to reduce statistical noise; accumulated profiles are superimposed with their mirror images with respect to this plane.

For the sake of comparison with the unconstrained bulk, some bulk fluid simulations were performed in the absence of walls, i.e., incorporating periodic boundary conditions in all three directions. The system volume, total number of chains, chain length, interaction energetics, and temperature were the same as in our interfacial work. The same elementary moves were employed, and the simulation algorithm is again described by eq 1–4, where, of course, all surface contributions are zero. A binning scheme was not implemented in our bulk simulations, since the model system was found to be isotropic in all three directions, as expected.

4. Results and Discussion

Equilibrium Structure. We discuss here the structure of our macromolecular fluid, confined between solid walls, in each of the three cases summarized in Table I. In the course of the equilibrium portion (stage 2) of each run, configurations were analyzed 1000 times, every $r^3 = 8000$ bead cycles. The local density distribution of segments, the spatial distribution of chain centers of mass, and chain shape characteristics were monitored.

An important length scale of the system is the root-mean-squared radius of gyration that the chains assume in the unconstrained bulk. Our value for this quantity was found to be 2.15 ± 0.01 lattice spacings from the bulk simulations. The volume fraction of segments is calculated as a function of distance from the wall by counting the total number of beads $n_s(z)$ and dividing by the total available number of cells $L = 49$ in each bin Z, centered at $z = (Z - {}^1/_2)l$:

$$\varphi(z) = n_s(z)/L \tag{7}$$

$\langle\varphi(z)\rangle$ for all three interfacial cases and for the unconstrained bulk is plotted in Figure 3. Results from cases I and II are identical, within the noise of the simulation. This is expected, since, as mentioned above, barriers to lateral motion on the surface affect dynamic characteristics, but not equilibrium thermodynamic and structural properties. Such a coincidence between cases I and II was observed in all our equilibrium results; results from case II will not be shown, therefore, until we come to the discussion of dynamics.

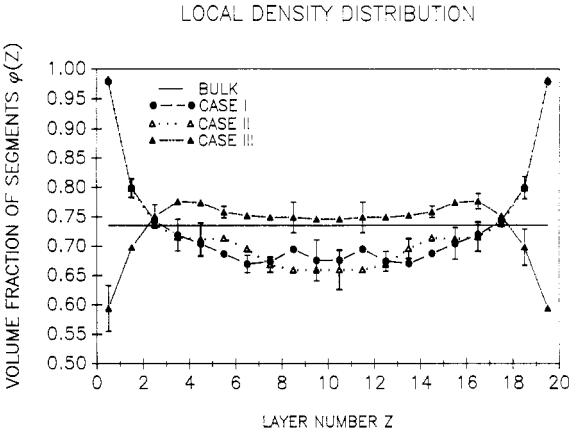

Figure 3. Spatial distribution of local segment density, in all cases studied. $\varphi(z)$ is the fraction of occupied cells in the lattice layer centered at z/l.

In the strongly adsorptive case I, chain segments concentrate preferentially at the surface. The local density falls off quasi-exponentially, over a distance of a few layers, to a constant value, characteristic of the central region between the plates. In case I, segment density at the system midplane falls slightly short of the unconstrained bulk density. This is due to the constant mass nature of the simulations; since both the interfacial and the bulk simulations were performed at a constant chain number-to-volume ratio, surface enhancement will necessarily be accompanied by middle region depletion with respect to the bulk. If the model film were infinitely thick, then the middle region would be indistinguishable from the unconstrained bulk.

Interestingly, in case III, where the solid surfaces attract polymer segments only weakly, exactly the opposite behavior is seen; there is a density depletion near the surface, and a slight enhancement relative to the bulk in the middle region. The waviness displayed by the profiles in Figure 3 is within the 95% confidence limits; no definite conclusions can be drawn, therefore, as to the existence of "fine structure" effects. Note that the artificial discretization inherent in the lattice model limits the possibility of observing layering phenomena in the vicinity of surfaces, although such layering may be present in real polymer melts.[7]

To explore local structure on a molecular, rather than on a segment basis, we computed the z component of the center of mass (COM) for each individual chain, according to the equation

$$\bar{z} = \frac{1}{r}\sum_{i=1}^{r} z_i \tag{8}$$

where z_i stands for the z coordinate of bead i in the considered chain. Each center of mass was then assigned to the appropriate layer or bin (we call such an assignment a "hit"), and a running total of hits per bin was maintained. Results were reduced by dividing the number of hits $H(Z)$ in a given bin Z by the number of hits per bin that would ensue from the hypothetical case of a uniform distribution

of COMs. The resulting quantity, given by eq 9, is es-

$$g^{(1)}_{COM}(z) = \frac{\rho_{COM}(z)}{\bar{\rho}_{COM}} = \frac{H(Z)}{\frac{1}{B}\sum_{Z=1}^{B} H(Z)} \quad (9)$$

sentially a singlet density distribution of centers of mass, normalized by its value in a bulk phase of the same average density. The $g^{(1)}_{COM}$ profiles for cases I and III are shown in Figure 4. As evidenced by the error bars, this is a slower converging property than the local segment density. In all cases, only a few chains have their COMs located directly adjacent to the surface; this is due to the steric exclusion of polymer by the solid surfaces. A significant peak is observed in the second layer from the wall, at a distance of slightly less than one unperturbed chain radius of gyration. The strongly adsorbing case I and the equivalent case II exhibit a more pronounced peak here than case III. All cases decay to an asymptotic value of practically 1 within only four layers from the wall. There is no indication of secondary or higher order peaks within our noise limits. Our observations are in qualitative agreement with Madden's[5] recent simulation of a longer chain system.

To assess perturbations in chain shape, induced by the presence of surfaces, we studied the segment distributions of individual chains as a function of the location of their centers of mass. Each time the progress of the simulation was monitored, chains were subdivided into $B = 20$ subcategories, according to the current locations of their centers of mass. For each subcategory, the fraction of beads lying within each bin of the lattice was determined. By maintaining running averages of these fractions, probability density functions, $f(z)$, were accumulated that describe the spatial disposition of the segment cloud of a chain, given its center of mass coordinate along the z direction. Results obtained in case I are presented in Figure 5, for a variety of COM locations. The probability density is defined to be zero at the walls. Only a few chain profiles are shown in the middle region; the profile there assumes an asymptotic form, which remains practically invariant with COM position, down to COM positions as close to the wall as $z/l = 5$. The bell-shaped appearance of $f(z)$ profiles in this middle region is a signature of unperturbed chains; indeed, conformations here are indistinguishable from those encountered in the unconstrained bulk. Near the solid surfaces, chain conformation departs drastically from its bulk behavior. Chains are pronouncedly flattened. To explore the sensitivity of this flattening tendency to the intensity of segment/solid interactions, we present a comparison of the three profiles closest to the wall between cases I and III in Figure 6. Only for chains with their center of mass in the first lattice layer is some difference observed. Here, the stronger adsorptive interactions characteristic of case I lead to a somewhat flatter profile. On the contrary, in case III adsorbed chains tend to protrude a few more segments into the energetically more favorable bulk domain. The reader should keep in mind that although profiles plotted in Figure 6 look quite similar between cases I and III, the actual population of chains with their COMs close to the surface is considerably lower in case III, as evidenced by Figure 4.

The structural observations on segment density distribution and chain shape summarized above are in agreement with the predictions of a recent mean field, variable density lattice model of polymer liquids at interfaces.[4]

Dynamic Properties. Apart from equilibrium structural features, our dynamic Monte Carlo simulations, when interpreted along the lines discussed in the Introduction,

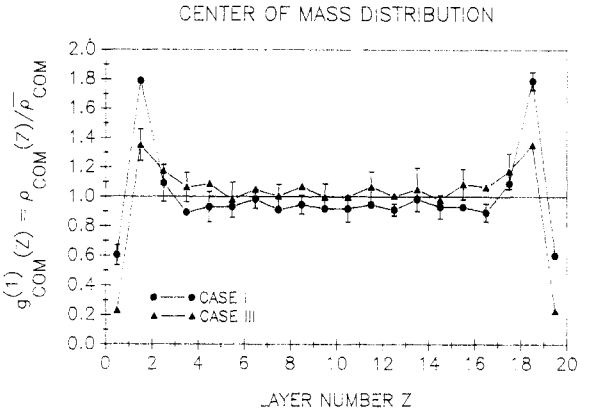

Figure 4. Chain center of mass (COM) distribution in cases I and III. $g^{(1)}_{COM}(z)$ is the number of COMs located in a given bin Z, centered at $z = (Z - 1/2)l$, divided by the number of COMs one would find in the same bin, if the COM distribution were spatially uniform.

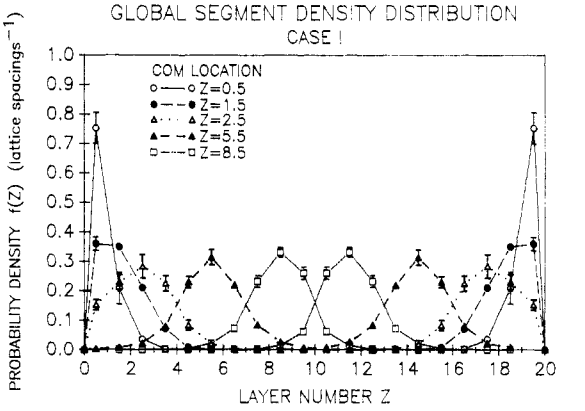

Figure 5. Spatial distribution of the segment cloud of individual chains as a function of their center of mass location in case I. $f(z)$ is the fraction of beads located in bin Z, centered at $z = (Z - 1/2)l$, for a chain with the indicated COM position.

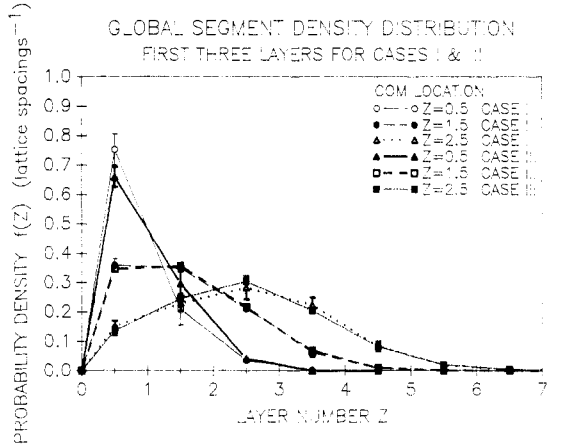

Figure 6. Detail of the segment distribution profiles for cases I and III. Only chains whose center of mass is located in the first bin ($z/l = 0.5$) show a small difference in shape between the two cases.

provide information on molecular mobility and relaxation under equilibrium conditions, which we will now examine. The value of these dynamic characterstics lies in that they are intimately related to the transport behavior our fluid will exhibit under nonequilibrium situations, such as flow. The rate of chain center of mass diffusion is proportional to fluidity, or inverse viscosity. The longest relaxation time provides an estimate of the rate at which chains will lose memory of their original conformational characteristics and hence of the viscoelastic effects to be expected when they

are subjected to external deformations at a rate commensurate with this intrinsic relaxation rate. Thus, in essence we are addressing the problem of how local viscosity and viscoelasticity in a liquid composed of chain molecules will be affected by the presence of adsorbing solid walls.

Dynamic information was collected in the course of the third stage of our simulation runs. At the beginning of this stage, a time was arbitrarily chosen as zero. The centers of mass and end-to-end vectors of all chains were recorded at this initial time and at 35 subsequent sampling times, separated from each other by $nr^2 = 14400$ bead cycles. We will refer to such a set of 36 consecutive samplings as a "time sweep". Upon completion of a time sweep, time was reset to zero, and a new sweep was initiated. Each simulation run contained a total of 600 such time sweeps, aimed at a detailed examination of chain mobility and relaxation.

As a measure of local mobility in our interfacial system we used the chain center-of-mass self-diffusion coefficient, D_T. This was calculated from our simulations as follows. First, the initial z component of the COM was found for every chain, using eq 8, and assigned to the appropriate bin. Next, during each of the 35 subsequent samplings, the positions of all COMs were recorded as functions of time. At the end of a time sweep the initial COM positions were updated, assigned to new bins, if necessary, and the tracking of COM displacement with time was continued for all chains. This procedure was repeated for a total of 600 time sweeps. Upon completion of a simulation run, squared COM displacement histories along each coordinate were averaged within each bin, over all chains whose initial COM positions were assigned to that bin during some time sweep. A plot of the squared COM displacement versus time (in bead cycles) reveals a curved portion at short times and a linear portion at long times. The self-diffusivity is determined from the slope of the linear region, by the Einstein relation

$$D_T = \frac{1}{6} \lim_{t\to\infty} \left[\frac{d\langle x^2 \rangle}{dt} + \frac{d\langle y^2 \rangle}{dt} + \frac{d\langle z^2 \rangle}{dt} \right] \quad (10)$$

It was established that the mean-squared displacements $\langle x^2 \rangle$, $\langle y^2 \rangle$, and $\langle z^2 \rangle$ were safely linear with time over samplings 18–36. The subscript T denotes total diffusive motion, in all three directions. Individual components of the diffusivity along the x, y, and z directions were also calculated from each of the individual terms on the right-hand side of eq 10:

$$D_X = \frac{1}{6} \lim_{t\to\infty} \frac{d\langle x^2 \rangle}{dt}$$

$$D_T = D_X + D_Y + D_Z \quad (11)$$

All diffusivities were obtained in units of l^2/τ.

The mean-squared displacement of chain COMs was also monitored as a function of time in our unconstrained bulk simulations; no bins were used in this case, since diffusion was found to be homogeneous and isotropic. The root-mean-squared displacement in the course of a time sweep was found to be 0.30 lattice spacings. This indicates that chain COMs do not depart significantly from their original position during a time sweep; it is therefore reasonable to classify local diffusive behavior in the interfacial systems in terms of the "bin" in which the center of mass lies at the beginning of a time sweep.

The total diffusivity D_T is plotted as a function of position for all three interfacial cases studied, as well as for the unconstrained bulk, in Figure 7. Near strongly adsorptive surfaces (cases I and II) self-diffusion is highly

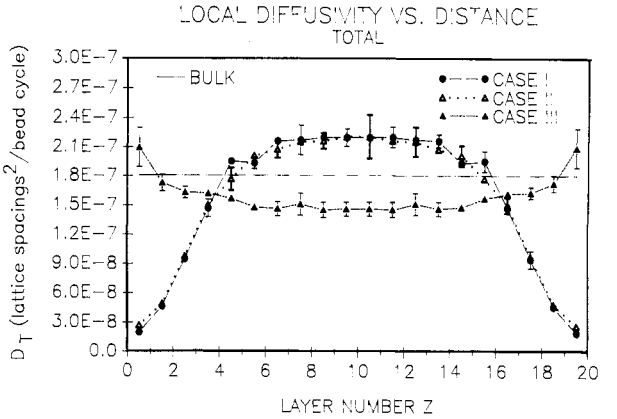

Figure 7. Total diffusivity of the chain center of mass, $D_T(z)$, as a function of center of mass location for cases I, II, and III and for the unconstrained bulk polymer.

hindered. It rises with increasing distance from the surface to a plateau value in the middle region, which exceeds that of the unconstrained bulk. A conclusion from the dynamic surface measurements of Horn and Israelachvili[2] is that the polymer has a viscosity equal to its bulk value throughout a thin film confined between strongly adsorbing walls, except for a region next to each surface, roughly one radius of gyration thick, where the polymer does not flow. Our diffusivity predictions for cases I and II are in very good agreement with this finding. In case III local diffusivity exhibits the exact opposite effect, being highest near the weakly adsorbing walls. Through comparisons against unconstrained bulk simulations, we have established that the departure of D_T from its bulk value in the middle region is due merely to the density differences discussed in conjunction with Figure 3. Diffusive behavior in the vicinity of solid walls is not exclusively governed by density effects, however; rather, it depends on the adsorptive strength and topography of the solid in subtle ways. A comparison of the curves plotted for cases I and II in Figure 7 indicates that barriers to the lateral motion of segments on the surface have only a small effect on the mobility of those chains whose COM is located very close to the solid. As discussed below, this effect results from a slowing down of molecular migration in the x and y directions rather than in the z direction.

To elucidate the anisotropic character of chain motion near an interface, we examined the separate components of diffusivity in each coordinate direction. In all cases, we find the components D_X and D_Y, parallel to the surface, to coincide for all layers. The D_Z component is indistinguishable from D_X and D_Y in the middle region for all cases, confirming that our model systems are dynamically isotropic there. D_Z departs substantially from D_X and D_Y near a wall, however. In the layer adjacent to the surface, D_Z was found to be less than D_X and D_Y by factors of roughly 2.5, 2.4, and 2.8 in cases I, II, and III, respectively. The relative magnitude of D_X, D_Y, and D_Z within various parts of the interfacial system in case III is characteristically seen in Figure 8: In the region next to the wall molecular migration is accelerated along the x and y directions (as would be expected by a density argument) but slowed down along the z direction, relative to the middle region. The solid straight line in Figure 8 indicates the value of self-diffusivity in an unconstrained bulk phase of the same average density as our interfacial system. D_Z components are compared across all three cases in Figure 9. They are identical between cases I and II and much higher in the weakly adsorbing case III near the surface. A comparison of the D_X component across all cases is

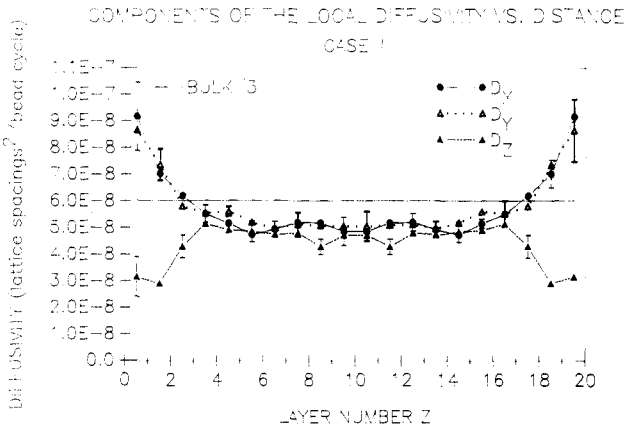

Figure 8. The three individual components of the self-diffusivity, $D_X(z)$, $D_Y(z)$, and $D_Z(z)$, plotted as functions of center of mass location in case III (weakly adsorbing surface). The value of these components in the isotropic bulk is also shown.

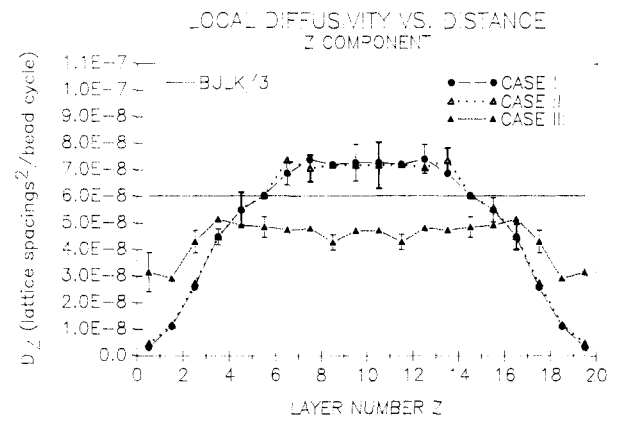

Figure 9. Center of mass diffusivity in the z direction, $D_Z(z)$, as a function of center of mass location in cases I, II, and III and in the unconstrained bulk polymer.

shown in Figure 10. Here the reduction in surface mobility, as one goes from cases I and II to case III, is even more pronounced. Also, there is some indication that surface barriers affect diffusivity. D_X next to the surface in case I is lower than in case II by a factor of 1.3, and this is outside the statistical noise of our simulations.

In summary, the overall effect of a strongly adsorbing surface is a decrease in total diffusivity over several layers close to the surface. Surface topography does not have a significant effect on center of mass diffusion. Near a weakly adsorbing surface, the mobility of chains is enhanced in directions parallel to the surface, mainly as a result of a decrease in polymer segment density.

A unique characteristic of macromolecular fluids is the ability of their constituent molecules to change shape continuously in the course of thermal motion. The characteristic times over which molecular sections of different lengths retain memory of their original orientation are very important material properties. They comprise a "spectrum of relaxation times", which is intimately related to the viscoelastic behavior exhibited by the polymer fluid under nonequilibrium conditions. To obtain a feeling of how molecular relaxation phenomena would be affected by the presence of adsorbing surfaces, we chose to examine the time over which the end-to-end vector loses memory of its original orientation as a function of position in the interfacial region. In the bulk, this time has been proved practically coincident with the relaxation time of the first normal mode of chains.[14] Following previous work[11] we will calculate this time via the autocorrelation function of the chain end-to-end vector, and we will call it the "longest

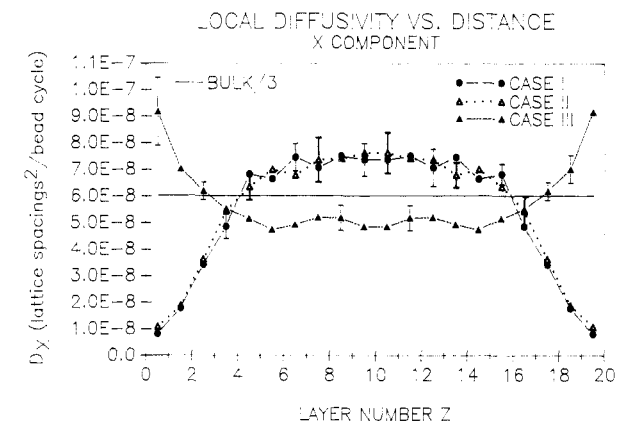

Figure 10. Center of mass diffusivity in the x direction (parallel to the surface), $D_X(z)$, as a function of chain center of mass location in cases I, II, and III and in the isotropic bulk.

relaxation time", τ_R. The autocorrelation function, $C_Z(t)$, was calculated again on the basis of the information accumulated in the course of the series of time sweeps performed during the dynamic portion (stage 3) of our simulation runs. At the start of a time sweep, the initial end-to-end distances of individual chains, $\mathbf{R}(0)$, were determined and assigned to bins, according to their initial COM positions. End-to-end vectors $\mathbf{R}(t)$ were computed and recorded for all chains during each of the subsequent 35 sampling times within a time sweep. A new time sweep was started by updating $\mathbf{R}(0)$ and rebinning chains with respect to their COM positions, if necessary. A total of 600 time sweeps were performed in a given run. The autocorrelation function was computed separately in each bin by

$$C_Z(t) = \langle \mathbf{R}(0)\cdot\mathbf{R}(t)\rangle_Z / \langle \mathbf{R}^2\rangle_Z \qquad (12)$$

The angular brackets in eq 12 symbolize an average over all chains whose COMs lay in bin Z at the beginning of any of the 600 time sweeps executed during a run. Individual $C_Z(t)$ curves were averaged for a second time, over all runs performed for a given case. In our relaxation work we will measure time t in multiples of $nr\tau$, which, as mentioned above, corresponds to a physical time interval that is independent of system size. We will refer to the ratio $t/nr\tau$ as time measured in "bead cycles per bead". A plot of the natural logarithm of C_Z versus $t/nr\tau$ displays a characteristic "relaxation" behavior. It is convex downward at short times but assumes a rectilinear form at long times. The longest relaxation time, $\tau_R(z)$, for each bin Z, centered at $z = (Z - {}^1/_2)l$, is simply found as the slope of the linear portion of such a plot:

$$1/\tau_R(z) = -\lim_{t\to\infty} \{\mathrm{d}[\ln C_Z(t)]/\mathrm{d}t\} \qquad (13)$$

To check our method of computing relaxation times, we performed a three-dimensional simulation on exactly the same bulk system studied previously by Kranbuehl and Schardt.[11] A comparison of our findings against theirs resulted in excellent agreement, as shown in Figure 11.

The natural logarithm of the autocorrelation function for five different center of mass locations (bins), as obtained from all our case I simulation runs, is plotted as a function of time in Figure 12. The corresponding curve for the unconstrained bulk fluid is also shown. Chains with COMs in bins centered at $z/l = 4.5$ to $z/l = 9.5$ differ only little in their relaxation behavior; therefore, only two autocorrelation plots are shown in this region. The curves were taken as linear for times longer than 300 bead cycles/bead, and the longest relaxation times $\tau_R(z)$ were calculated from their slope in that region. We note that

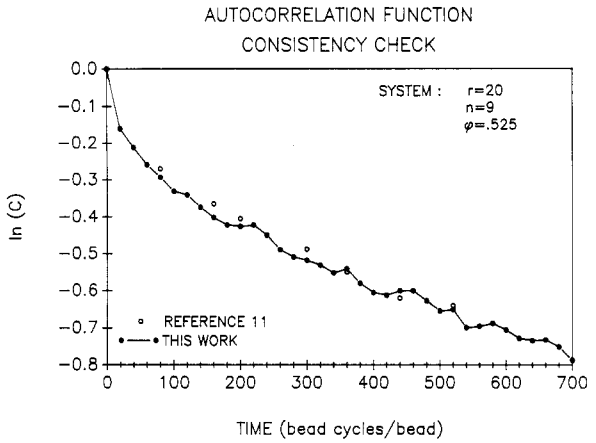

Figure 11. Logarithm of the end-to-end vector autocorrelation function plotted against dimensionless time, $t/nr\tau$, in bead cycles per bead, as obtained in this work and in the bulk simulation of Kranbuehl and Schardt. The test system consists of $n = 9$ chains of length $r = 20$ beads each, within a $7 \times 7 \times 7$ cubic lattice, characterized by periodic boundary conditions in all three directions. The volume fraction occupied is $\varphi = 0.525$.

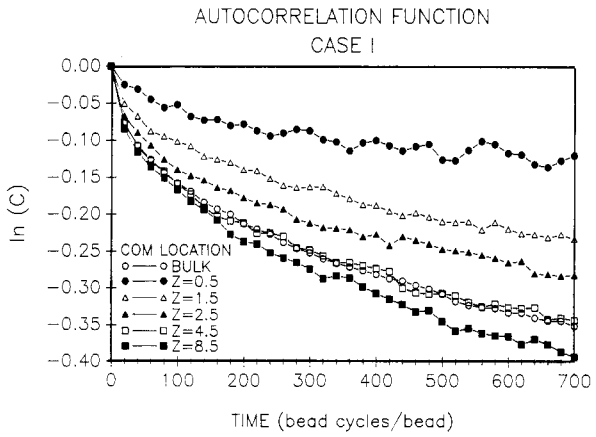

Figure 12. Natural logarithm of the end-to-end vector autocorrelation function plotted against dimensionless time, $t/nr\tau$, for chains with different center of mass positions in the interfacial system. Results from a simulation of the unconstrained bulk are also shown. The curves displayed here were obtained with the parameters of case I. Similar plots were constructed for cases II and III.

$\tau_R(z)$ is subject to considerable statistical error, especially near the surface, where few chains are located (compare Figure 4).

Graphs similar to those of Figure 12 were prepared for all three cases examined, and the corresponding $\tau_R(z)$ values determined. Results on τ_R as a function of position are plotted in Figure 13; error bars indicate 95% confidence limits. A first interesting observation is that, next to the wall, case I chains have a much longer relaxation time than case II chains. In other words, barriers to the lateral motion of beads exert a pronounced influence on chain relaxation near the surface. The surface relaxation time $\tau_R(l/2)$ is longer in case II than in case III, which in turn exhibits a longer $\tau_R(l/2)$ than the unconstrained bulk. The presence of the solid affects relaxation over a region approximately three lattice layers wide. A slight dip in $\tau_R(z)$ is apparent in all three cases at $z/l = 1.5$, i.e., at the same location where the center of mass distribution of Figure 4 is sharply peaked. This dip is particulaly evident in case III. Differences between the three cases in the asymptotic middle region between the plates are small. In this region, cases I and II exhibit a somewhat faster and case III a somewhat slower relaxation than the unconstrained bulk. This is again purely a density effect, encountered in all of our dynamic results.

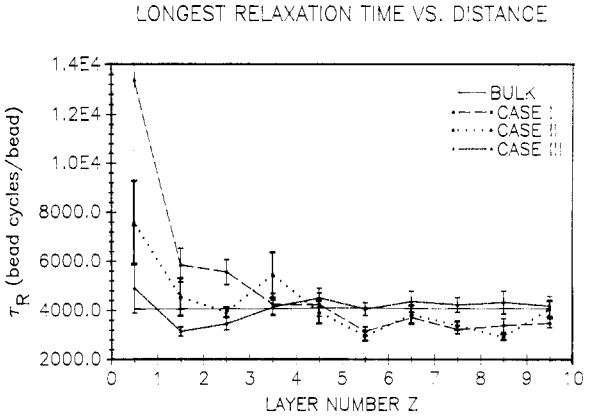

Figure 13. Longest relaxation time $\tau_R(z)$, in units of $nr\tau$ (see text) as a function of chain center of mass position z in cases I, II, and III.

Our simple lattice Monte Carlo simulations have led to some interesting observations regarding the dynamic behavior of chains near surfaces. A solid surface can be characterized in terms of the depth of attractive energy wells that it presents to the segments of a chain molecule and in terms of the height of the energy barriers separating these wells. Even if barriers do not affect equilibrium thermodynamic and structural characteristics, they inhibit lateral mobility on the surface at the level of individual segments. Barriers were found to exert a pronounced influence on the relaxation behavior of adsorbed chains. As seen in Figure 5, the shapes of adsorbed chains are flattened near strongly adsorbing surfaces, with a large percentage of segments directly adsorbed on the surface. In addition, recent analytical work[4] indicates a tendency of chain ends to expose themselves preferentially to the surface, which was confirmed by these simulations (results not shown here). The above aspects of structure cause the longest relaxation time, defined in terms of the rate at which the end-to-end vector loses memory of its original orientation, to rise in the presence of surface barriers. In contrast to their role in relaxation, barriers do not have a serious effect on translational mobility (self-diffusion), at the level of the entire chain. The latter seems to be dominated by the intensity of solid/segment interactions and by the density profile that develops as a result of these interactions in the interfacial region. Chain self-diffusion is very slow near strongly adsorbing surfaces, in comparison to the unconstrained bulk.

5. Summary and Conclusions

Dynamic Monte Carlo simulations have been performed on a dense multichain system in the vicinity of walls to elucidate the equilibrium structure, as well as the dynamic behavior of a polymer/solid interface. Three cases have been studied: (I) a highly adsorptive surface with strong intersite potential barriers that inhibit lateral motion along the surface; (II) a highly adsorptive surface with no potential barriers; (III) a weakly adsorptive surface with weak intersite barriers.

It has been discovered that walls significantly alter local structure and conformation, over a region several layers from the surface, even though segment/solid and segment/segment interactions have been confined to nearest-neighbor cells. Segment density is enhanced near strongly adsorbing surfaces and depleted near weakly adsorbing surfaces. The spatial distribution of chain centers of mass exhibits some structure, as a result of entropic constraints to chain propagation imposed by solid walls. Chain shapes are pronouncedly flattened in the vicinity

of the solid surface. These results are in general agreement with previous Monte Carlo simulations[5-7] and with predictions of an analytical mean field theory.[3,4]

The dynamic behavior of chains near surfaces has been studied for the first time in this work. Two aspects of dynamics have been examined. First, the chain center of mass self-diffusivity was evaluated as a function of position in the interfacial region and found to be strongly related to local density near a surface. Diffusive motion is intrinsically anisotropic; it is slower in directions perpendicular than in directions parallel to the surface, in all cases examined. Strong segment adsorption slows down self-diffusion quite substantially. On the contrary, intersite energy barriers, which suppress local segmental motion, do not seem to exert a pronounced influence on the self-diffusivity of entire chains near strongly attractive walls. A second dynamic aspect examined in this work was the longest relaxation time of chains, defined in terms of the decay in the autocorrelation function of the end-to-end vector. The variation of longest relaxation times with center of mass position has been explored. Strong segment adsorption leads to longer relaxation times in the vicinity of the surface. In addition, it has been discovered that high intersite barriers prolong chain relaxation near attractive walls very significantly.

Computations aimed at exploring the effects of higher densities, longer chains, and "crankshaft" moves on interfacial structure and dynamics are in order. It must be emphasized that this work refers to relatively short chains, and therefore only tentative conclusions can be drawn about the dynamic behavior of high molecular weight polymer melts, where chain entanglements may be a dominant factor.

Acknowledgment. This work was supported by the Director, Office of Energy Research, Office of Basic Energy Sciences, Materials Science Division of the U.S. Department of Energy, under Contract No. DE-ACO3-76SF00098. We express sincere gratitude to Cray Research, Inc., for the award of Cray X-MP/48 time under a 1987 and 1988 University Research and Development Grant and to the San Diego Supercomputer Center, where some of our calculations were performed. D.N.T. thanks the National Science Foundation for a Presidential Young Investigator Award, No. DMR-8857659. We also thank Professors Michael C. Williams and Morton M. Denn for many stimulating and enlightening discussions.

References and Notes

(1) Ramamurthy, A. V. *J. Rheol.* **1986**, *30*, 337.
(2) Horn, R. G.; Israelachvili, J. N. *Macromolecules* **1988**, *21*, 2836.
(3) Theodorou, D. N. *Macromolecules* **1988**, *21*, 1391, 1400.
(4) Theodorou, D. N., manuscript in preparation.
(5) Madden, W. G. *J. Chem. Phys.* **1987**, *87*, 1405; **1988**, *88*, 3934.
(6) Ten Brinke, G.; Ausserrē, D.; Hadziioannou, G. *J. Chem. Phys.* **1988**, *89*, 4374.
(7) Kumar, S. K.; Vacatello, M.; Yoon, D. Y. *J. Chem. Phys.* **1988**, *89*, 5206.
(8) Metropolis, N.; Rosenbluth, A. W.; Rosenbluth, M. N.; Teller, A. H.; Teller, E. *J. Chem. Phys.* **1953**, *21*, 1087.
(9) Kremer, K.; Binder, K. *Comput. Phys. Rep.* **1988**, *7*, 259.
(10) Verdier, P. H.; Stockmayer, W. H. *J. Chem. Phys.* **1962**, *36*, 227.
(11) Kranbuehl, D. E.; Schardt, B. In *Computer Modeling of Matter*; Lykos, P., Ed.; ACS Symposium Series No. 86; American Chemical Society: Washington, D. C., 1978; pp 125–136.
(12) Binder, K. In *Monte Carlo Methods in Statistical Physics*; Binder, K., Ed.; Springer-Verlag: Berlin, 1979; pp 1–45.
(13) Crabb, C. C.; Kovac, J. *Macromolecules* **1985**, *18*, 1430.
(14) Dial, M.; Crabb, K. S.; Crabb, C. C.; Kovac, J. *Macromolecules* **1985**, *18*, 2215.
(15) Hilhorst, H. J.; Deutch, J. M. *J. Chem. Phys.* **1975**, *63*, 5153.
(16) Verdier, P. H.; Kranbuehl, D. E. *Macromolecules* **1987**, *20*, 1362.
(17) Naghizadeh, J.; Kovac, J. *Phys. Rev. B* **1986**, *34*, 1984.
(18) Naghizadeh, J.; Kovac, J. *Phys. Rev. Lett.* **1987**, *59*, 1710.
(19) Romiszowski, P.; Stockmayer, W. H. *J. Chem. Phys.* **1984**, *80*, 485.
(20) Downey, J. P.; Crabb, C. C.; Kovac, J. *Macromolecules* **1986**, *19*, 2202.
(21) Sanchez, I. C.; Lacombe, R. H. *J. Chem. Phys.* **1976**, *80*, 2352; *J. Polym. Sci., Polym. Lett. Ed.* **1977**, *15*, 71; *Macromolecules* **1978**, *11*, 1145.
(22) Crabb, C. C.; Hoffman, D. F., Jr.; Dial, M.; Kovac, J. *Macromolecules* **1988**, *21*, 2230.
(23) Kolinski, A.; Skolnick, J.; Yaris, R. *J. Chem. Phys.* **1987**, *86*, 7164.
(24) Stokely, C.; Crabb, C. C.; Kovac, J. *Macromolecules* **1986**, *19*, 860.
(25) Owicki, J. C. In *Computer Modeling of Matter*; Lykos, P., Ed.; ACS Symposium Series No. 86; American Chemical Society: Washington, DC, 1978; pp 159–171.
(26) Pangali, C.; Rao, M.; Berne, B. J. *Chem. Phys. Lett.* **1978**, *55*, 413.
(27) Tsikoyiannis, J. G. Ph.D. Thesis, Department of Chemical Engineering, Massachusetts Institute of Technology, 1986.
(28) Ertl, H.; Dullien, F. A. L. *AIChE J.* **1973**, *19*, 1215.